(NASA-CR-142302) INVESTIGATIONS OF THE LUNAR SURFACE Status Report, 1 Mar. 1974 - 31 Mar. 1975 (Arizona Univ., Tucson.) 36 p HC $3.75 CSCL 03B

N75-19110

Unclas G3/91 13369

Investigations of the Lunar Surface

NGL 03-002-191

Status Report
1 March 1974 - 31 March 1975

R. G. Strom
E. Whitaker
L. Andersson

DEPARTMENT OF PLANETARY SCIENCES

LUNAR AND PLANETARY LABORATORY

UNIVERSITY OF ARIZONA
TUCSON ARIZONA 85721

Status Report

for the period 1 March 1974 - 31 March 1975

to

National Aeronautics and Space Administration

Lunar and Planetary Laboratory
University of Arizona

Research Grant NGL 03-002-191

(Investigations of the Lunar Surface)

by

Robert G. Strom
Associate Professor

Ewen Whitaker
Research Associate

Leif Andersson
Research Associate

Application is hereby made for continued step-funding support for the scientific programs in lunar research at the Lunar and Planetary Laboratory.

A. Lunar Photographs and Maps Collection

This has been augmented by the acquisition of Apollo 17 metric camera photography, also of the published sheets of the DMA Lunar Topographic Orthophotomap series. Prospects for housing the entire collection of lunar and planetary imagery and maps in one secure location are now promising. It is hoped to obtain a computerized microfiche reader to simplify retrieval operations. Very recently, an offer has been received from the new Main Library of the University, which is nearly completed and is situated close to LPL, to house this collection in a secure location there with librarian services provided gratis. However, the pros and cons of this offer will be examined very closely before any commitment is made.

B. Personnel

Lydia Chen and Sheryl Vrba have continued the crater cataloguing, measurement, and supporting card-punching operations under the immediate supervision of Leif Andersson, who has also been responsible for the thorough checking of all catalogued data, and the production of the important and fundamental statistics given later in this application. He has also re-written the crater-depth program (copy of method appended), prepared a program which produces coordinate grids for any Orbiter photograph, and written several other computer programs for processing the crater data. He obtained his PhD degree from Indiana University in September 1974.

Bruce Cordell, a graduate student in the Department of Planetary Sciences, is doing theoretical work relating to the modification of the diameter/frequency distribution of craters by basin ejecta, and is comparing the resulting expressions with crater counts from the new catalogue.

Ralph Turner has completed all work on the model of Schröter's Valley, and has provided us with a fully illustrated report which only needs editing prior to publication.

C. Scientific Programs

1. Crater Measuring and Statistical Program

General Status. It has been decided to publish the lunar crater catalogue in two volumes: one containing the earthside measurements and the other containing the farside measurements. These volumes will appear as Contributions of the LPL, since the material is too bulky for publication in the standard journal literature.

To date measurements of over 17,000 craters have been completed. The entire earthside hemisphere is almost ready for publication and is expected to be in press by early summer. Only checking of a small part of the limb regions and the addition of a new piece of information (presence of a ray system) need to be completed. The number of craters measured on the earthside is about 11,800. The positions of about 1,000 craters very near the limb as listed in the old catalogue have been found to be seriously in error. These positions are currently being corrected. The outline maps and indices for the earthside are almost ready and will require only a little additional time to complete.

The previously used depth calculation procedure has been replaced by a more exact one (Appendix I), prepared by Leif Andersson, and the photographic supporting data used in these calculations have been updated. Depths for all craters with measured shadows are being recalculated using the new procedure and the updated photo data. Therefore, the catalogue of crater depths published by Arthur (1974), which was based on measurements made at LPL, does not give the best values available for these craters.

About 40% of the farside has been measured and most of these craters (over 5,000) are already on punched cards. Since much of the best available photography of the farside is at a rather small scale, only selected

parts (about 50%) will be measured to the same nominal limit of completeness (7 km) as the earthside; the rest will be complete to 10 km diameter. When completed, about 13,000 craters will have been measured on the farside. We had intended to use the farside coordinate grids from ACIC for crater positions. However, these have not been forthcoming and therefore Leif Andersson has prepared a computer program which generates these grids using the updated photo data. The program is very flexible and is also used to plot crater diameters on an overlay for any given photograph. This provides an extremely accurate and efficient method of checking crater positions and diameters.

Preliminary Results. As stated in previous reports, crater depths based on the new measurements are significantly greater (often by 50-100%) than those calculated from earthbased measurements. Confirmation of these depths has recently been made by Pike (1974) using photogrammetric methods on limited numbers of craters contained on the Apollo metric camera photographs. As shown by Figures 1-5, the depth-diameter ratio for craters less than about 25 km in diameter is fairly constant and well defined for each age class (Class 1 is youngest, 5 oldest), indicating that the age classification is basically correct.

The diameter/frequency distribution of farside craters measured to date suggests that at least the central farside has a significantly higher crater density (~1.5) than typical southern highlands on the earthside (Figure 6). This is evident for all crater sizes of Classes 1 through 3. This suggests that the paucity of craters in this area of the earthside highland is not due to nearby basin formation since this would have preferentially obliterated the smaller craters with respect to the larger. The investigation of the number density of craters in selected areas of the highlands will be very valuable in evaluating possible causes of these differences.

Fragmentation theory predicts that the log frequency versus log diameter plot for impact craters should show a -2 slope. The most widely referenced earlier crater counts are those of Hartmann (1966, 1967) which seemed to confirm the -2 slope. These counts in highland areas were based on the old LPL crater catalogue and on early Lunar Orbiter photos of the farside. Furthermore, the counts were made in selected areas of the highlands (termed "Pure Uplands") which show high crater densities and were considered to be equilibrium surfaces. The counts on the frontside show a slight downward bend below about 60 km, but when combined with the farside data the best fit seemed to be a straight line with a -2 slope. Hartmann then compared this -2 slope with crater counts for the heavily cratered provinces on Mars and reached rather fundamental conclusions concerning an episode of atmospheric erosion on Mars.

Figures 7 and 8 are diameter/frequency plots of the Hartmann counts for the Moon and Mars, Gault's counts for the cratered terrain on Mercury, and the new LPL counts for the lunar highlands based on the entire earthside and 40% of the farside. Our lunar data are much more complete than Hartmann's and represent a large homogeneous sample of highlands rather than selected areas. Figure 7 is the traditional diameter/frequency plot using logarithmic increments, while Figure 8 is a log-log plot of diameter versus relative crater density in craters per diameter squared of the different size increments. In Figure 8 these curves are referenced to Hartmann's -2 slope which is shown as a horizontal line. This type of plot shows much more graphically and realistically the differences and similarities between the curves, and significant departures from a -2 slope. The new lunar highland curve shows several new and far-reaching results.

Within the diameter limits of the data (7-450 km) the lunar highland counts do not conform to a -2 slope. The peak density occurs at about 80 km

and shows a significant decrease in density at diameters both below and above this value. If Hartmann's data points for the nearside and farside are examined separately, this same trend is seen in both sets of data. As previously mentioned, our data suggest that the crater density in almost all size ranges is greater on the farside highlands than the earthside highlands. Furthermore, our farside highlands data alone (Figure 6) clearly show a decrease in relative density below about 70 km in diameter when referenced to a -2 slope. We believe that when Hartmann combined his nearside data with the higher density farside, the general crater density was raised and the downturn of the curve was masked to give a "best fit" of all data to a -2 slope. The decrease in density below about 80 km in diameter shown on our curve may be due to obliteration of craters caused by basin formation and/or an early period of highland volcanism, or it may represent the size distribution of the impacting bodies. The apparent paucity of craters in the size range about 80-450 km may be due to one or more of the following: (1) extensive slumping in the larger craters and multi-ring basins thereby causing a larger diameter than the true excavation diameter, (2) a different population of large impacting bodies, or (3) the influx of large bodies being confined to an early history and then subsequently obliterated by later impacts and volcanism. When other statistical parameters in the catalogue are taken into account it may be possible to eliminate several of these alternatives.

Very significant is the fact that all three bodies (Moon, Mars and Mercury) show the same general shape of the crater diameter/frequency distribution. This indicates that the general cratering and subsequent modification histories are similar. Furthermore, the similarity between the lunar and martian curves indicates that the decrease in crater density below 60 km on

Mars is not solely the result of an episode of atmospheric erosion as proposed by Hartmann. As seen in Figure 8 the crater density of Mars is at least a factor of 2 less than that of the Moon at all sizes. If this crater density difference is taken into account, then the loss of craters between about 50 and 7 km diameter due to atmospheric erosion on Mars is only a factor of 1-2. This is considerably less than the factor of 2-18 for the same diameter range given by Hartmann's lunar and martian curves. These preliminary results are being prepared for publication.

It is clear from the preceding discussion that crater parameters for the entire Moon are required to adequately portray its cratering and subsequent modification history. Furthermore, these data are essential before reliable comparisons can be made with other planetary bodies.

2. Schröter's Valley Model

The contouring of the entire model by computer techniques was completed late in 1974, and Figure 9 is a much reduced copy of the assembled mosaic, presented in a Mercator projection. Absolute altitudes correspond to the best fit with data from DMA chart LT038B3, which overlaps a small area of the model. The depth of the Valley in this area is approximately 600 m both from the model and the DMA chart; this gives one some confidence in the general modeling technique used.

Cross sections in N-S and E-W directions, as well as height profiles along the Valley are given. These show very graphically the gradually decreasing downwards slope from the "Cobra Head" to the "tail", and the general slopes at specific locations (Figure 10). Arguments have been advanced for supposing that the narrow ends of sinuous rilles may be higher, thus resembling terrestrial rivers, with the flowing material draining down the crater at the broad ends. The model shows that this is certainly incorrect for Schröter's Valley, and by analogy, for other sinuous rilles.

3. 61-inch Color Filter Photography.

Mr. Whitaker was able to pursue this project actively for a period late in 1974, allowing relative calibration of the original films obtained with the 61-inch telescope. Methods of exposure and processing (with the LPL Transflo processor) of the intermediate positive transparencies were standardized to produce gamma (i.e. contrast) curves of the requisite shape and slope for any of the film pairs. It soon became apparent that with absolute calibration, the original films could yield reliable color and albedo values in addition to the color boundaries. A preliminary attempt was made in late March to make such calibrations, using a Pritchard photometer (kindly made available by Dr. L. Dunkelman of GSFC) attached to the 61-inch reflector. The results look very promising, and may already be suitable to calibrate the original images.

With both albedo and relative color data available, it will be possible to prepare a two dimensional plot which will segregate different units much more effectively than by color alone.

Figure 11 is a color-difference photograph of the Aristarchus region, showing the degree of resolution obtainable by combining photos. A comparison between this image and several other data sets (radar, IR, geology, etc.) was made

late in 1974 in conjunction with members of the S217 and S222 Lunar Synthesis Teams. The results were presented at the Sixth Lunar Science Conference, by S. Zisk and will be published in due course.

This project was funded separately last year (NSG 7014), but expected expenditures to complete project are sufficiently small to include them in this proposal.

REFERENCES

Hartmann, W. K., Early lunar cratering, Icarus, vol.5, 406-418, 1966.

Hartmann, W. K., Martian cratering, Icarus, vol.5,565-576, 1966.

Hartmann, W. K., Lunar crater counts.II: Three lunar surface type-areas, Comm.LPL, vol.6, no.81, 39-41, 1967.

Hartmann, W. K., Martian cratering, 4, Mariner 9 initial analysis of cratering chronology, J.Geophys.Res., vol.78, no.20, 4096-4116, 1973.

Murray, B. , et al., Mercury's surface: Preliminary description and interpretation from Mariner 10 pictures, Science, 185, 12 July 1974.

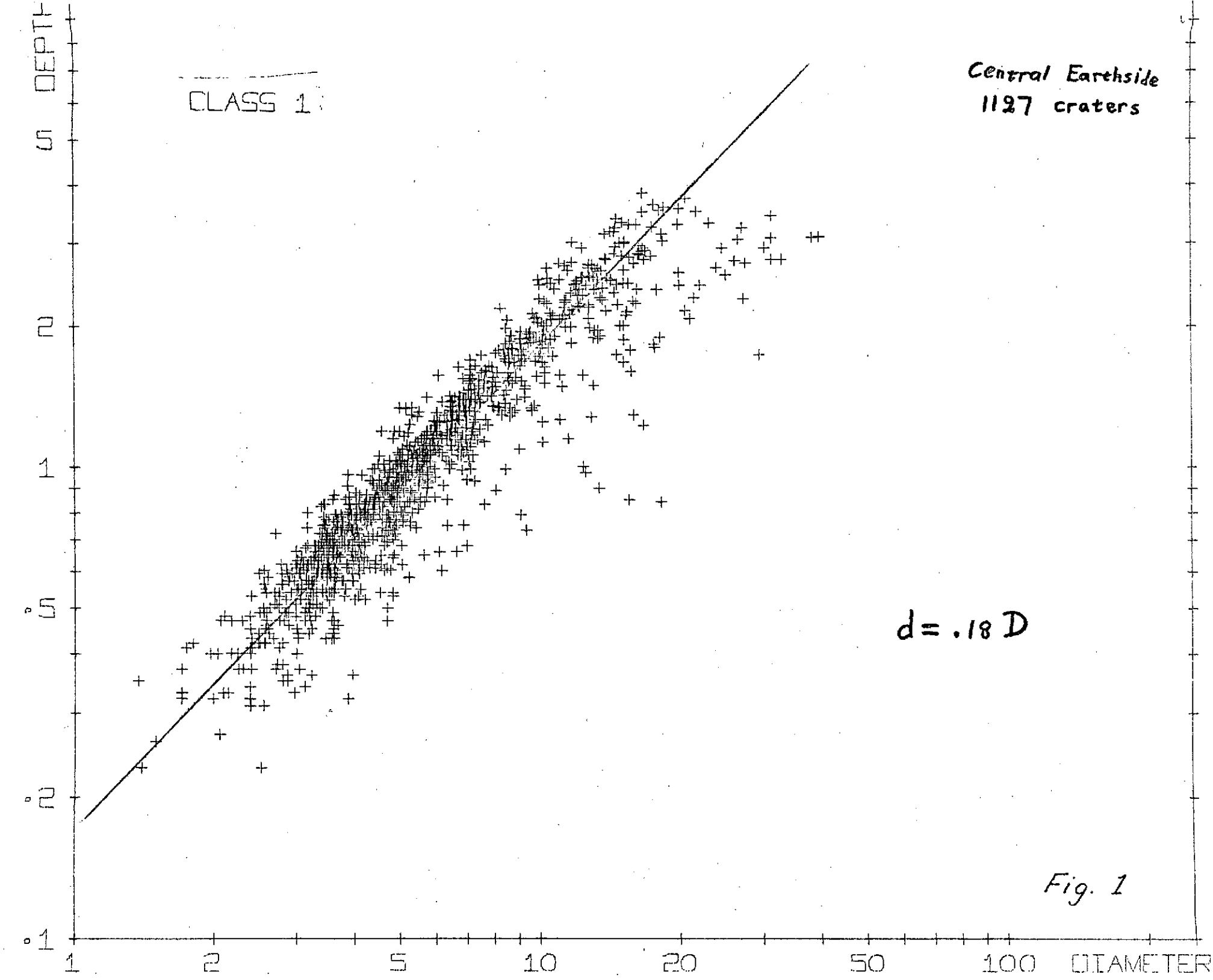
CLASS 1
Central Earthside
1127 craters
d = .18 D
Fig. 1
1
2
5
10
20
50
100
DIAMETER

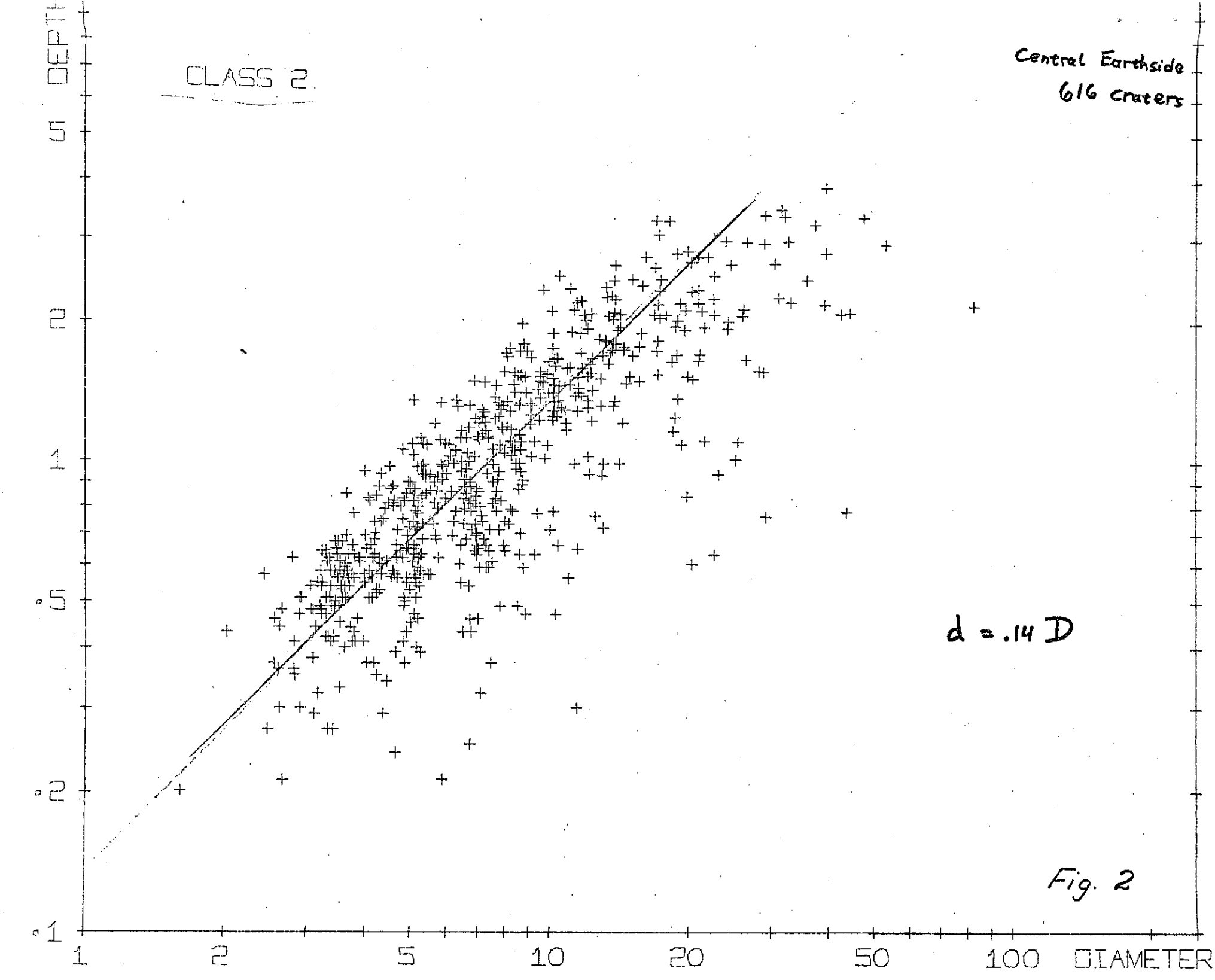
CLASS 2
Central Earthside
616 craters
d = .14 D
DEPTH
DIAMETER
1
2
5
10
20
50
100

Fig. 2

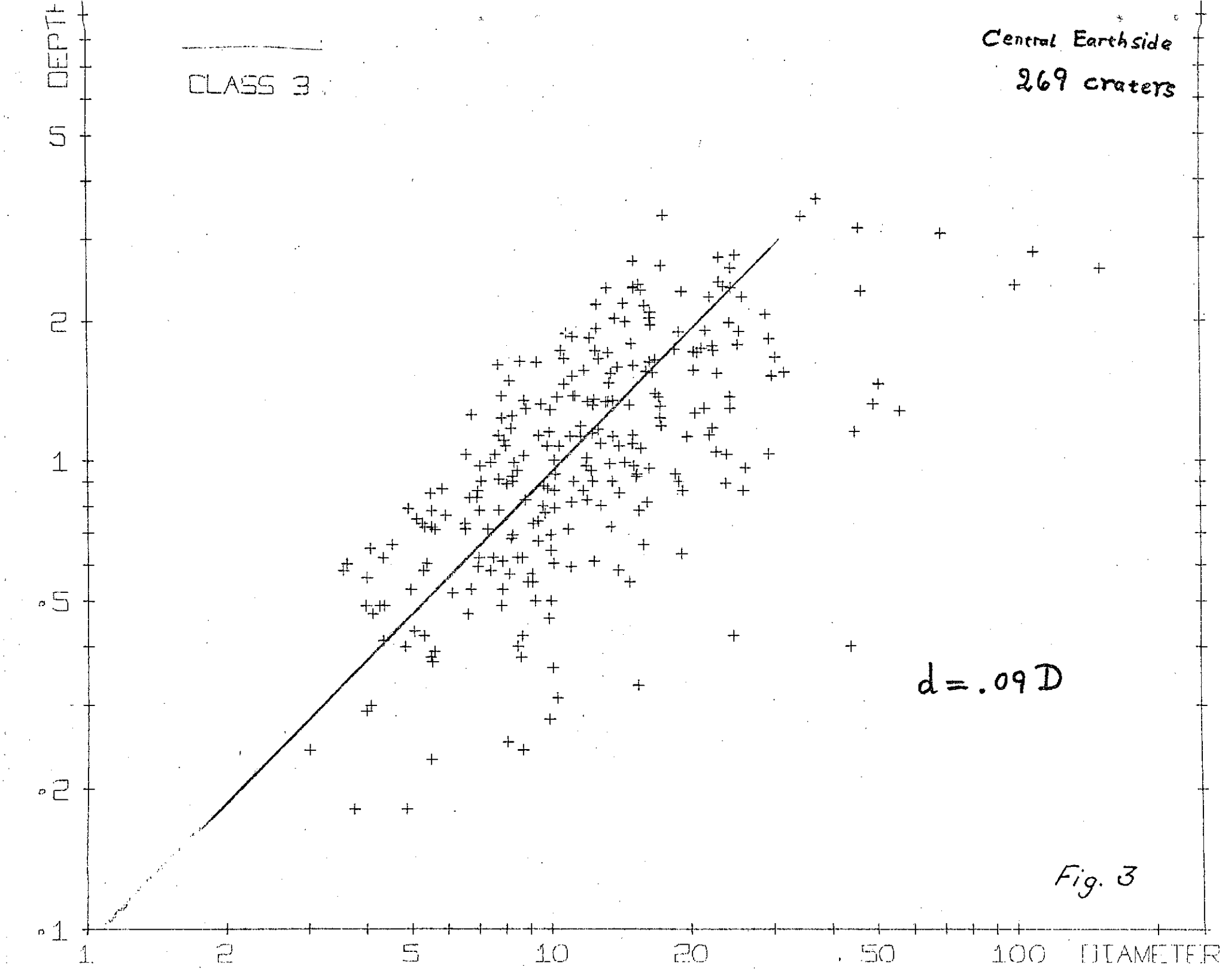
CLASS 3
Central Earthside
269 craters
d = .09 D
Fig. 3
DEPTH
DIAMETER
1
2
5
10
20
50
100

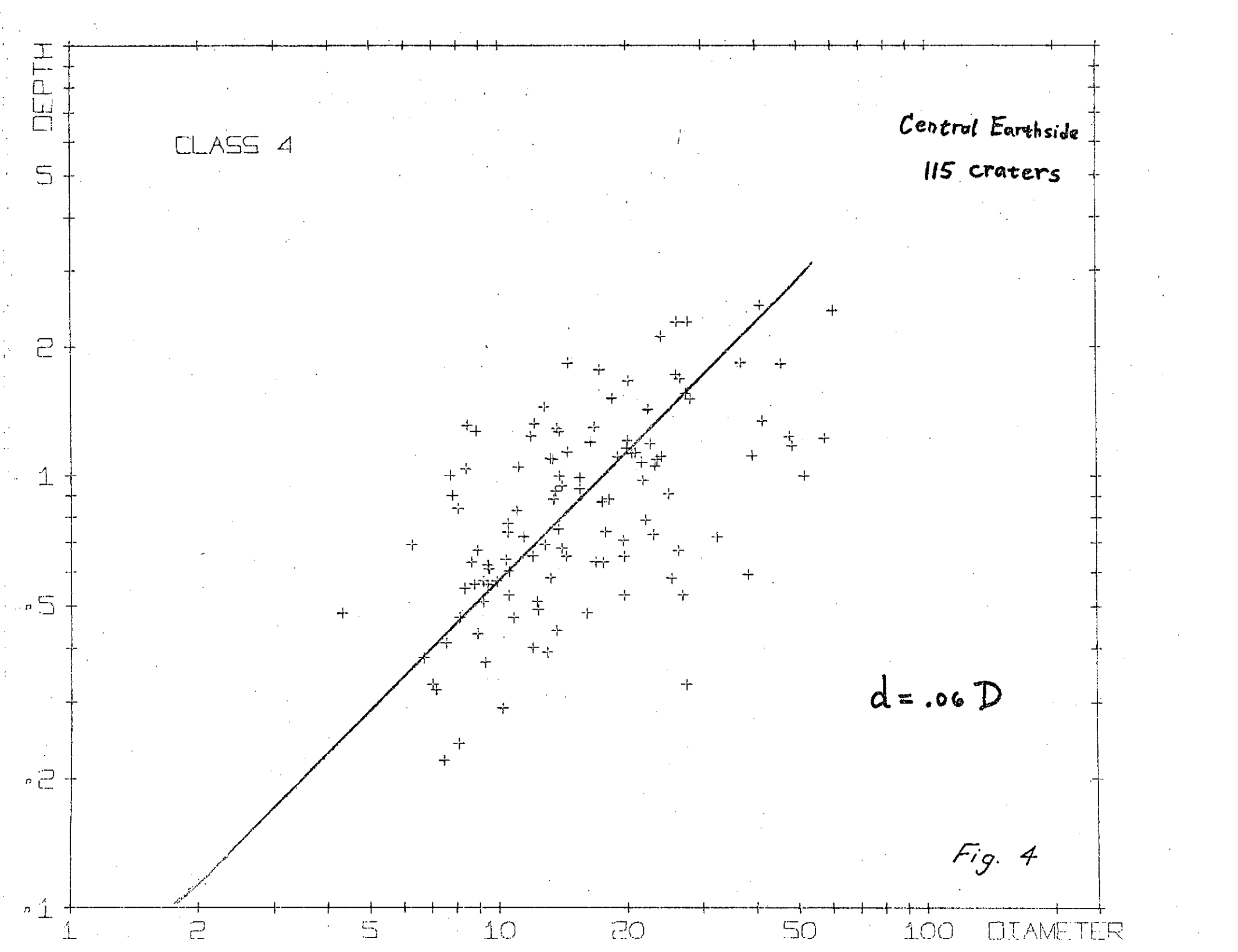
CLASS 4
Central Earthside
115 craters
d = .06 D
Fig. 4
DEPTH
DIAMETER
1
2
5
10
20
50
100

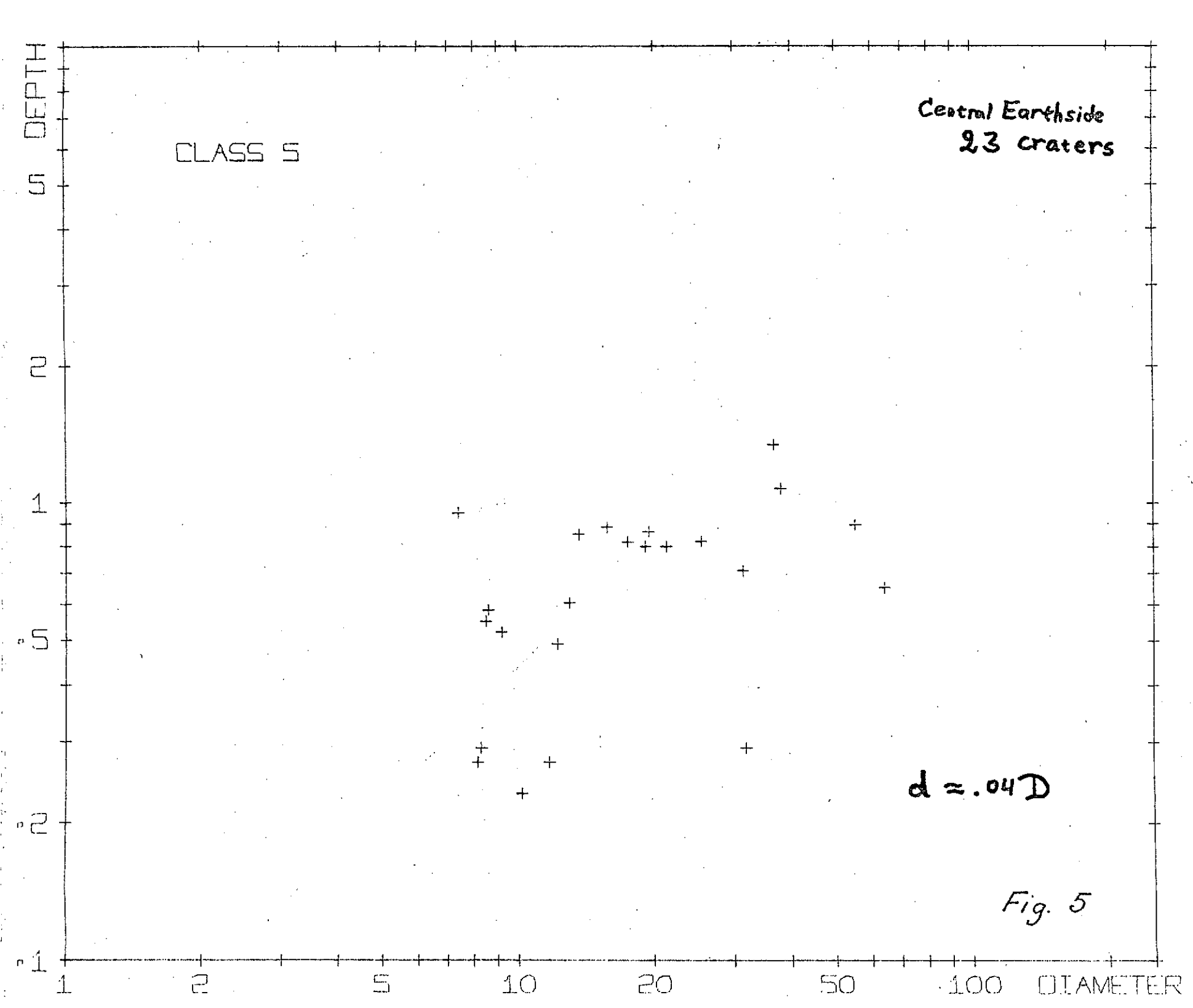
CLASS 5
Central Earthside
23 craters
d ≈ .04D
DEPTH
5
2
1
.5
.2
.1
1
2
5
10
20
50
100
DIAMETER

Fig. 5

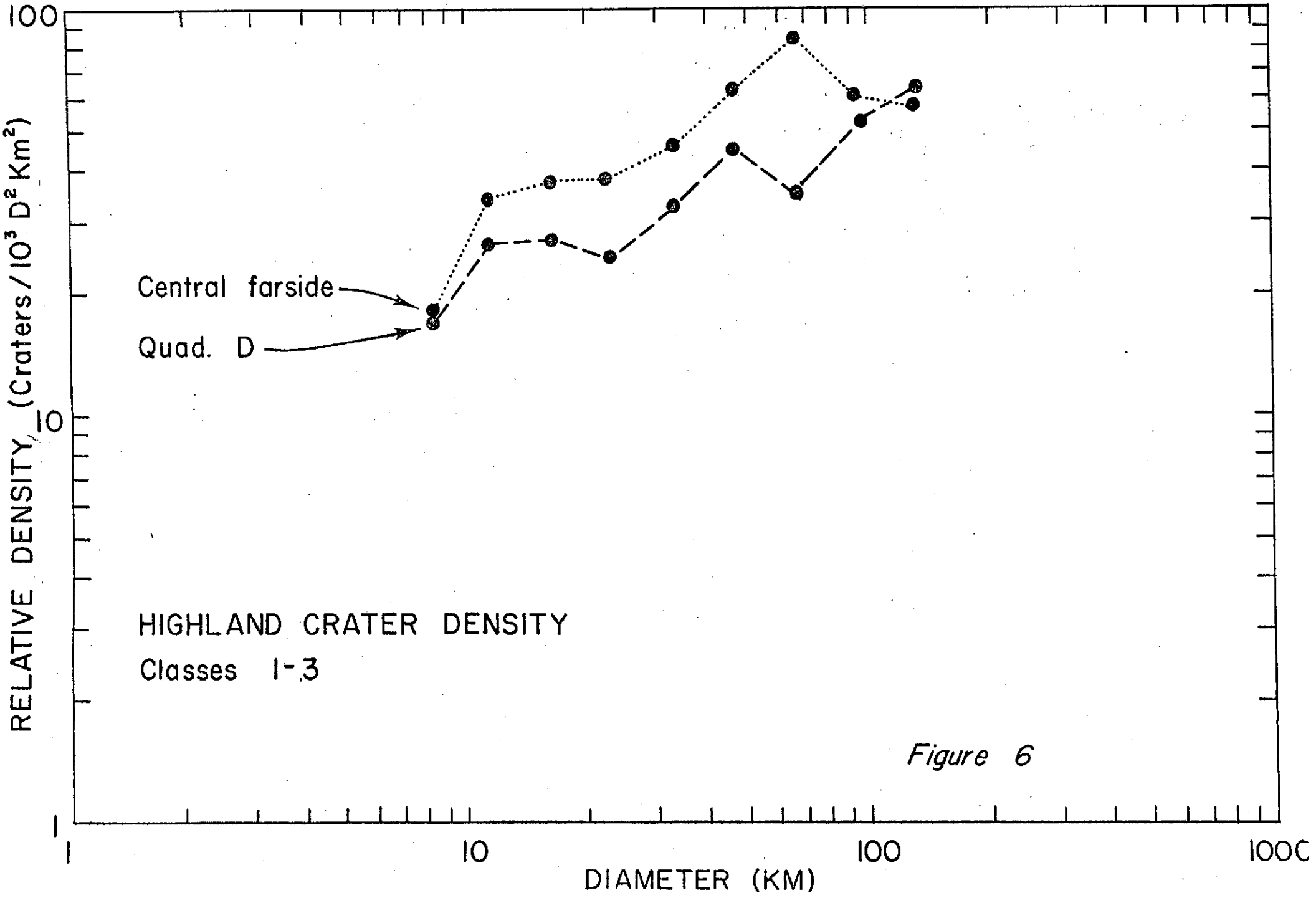
100
10
1
RELATIVE DENSITY (Craters / 10^3 D^2 Km^2)
Central farside
Quad. D
HIGHLAND CRATER DENSITY
Classes 1-3
1
10
100
1000
DIAMETER (KM)

Figure 6

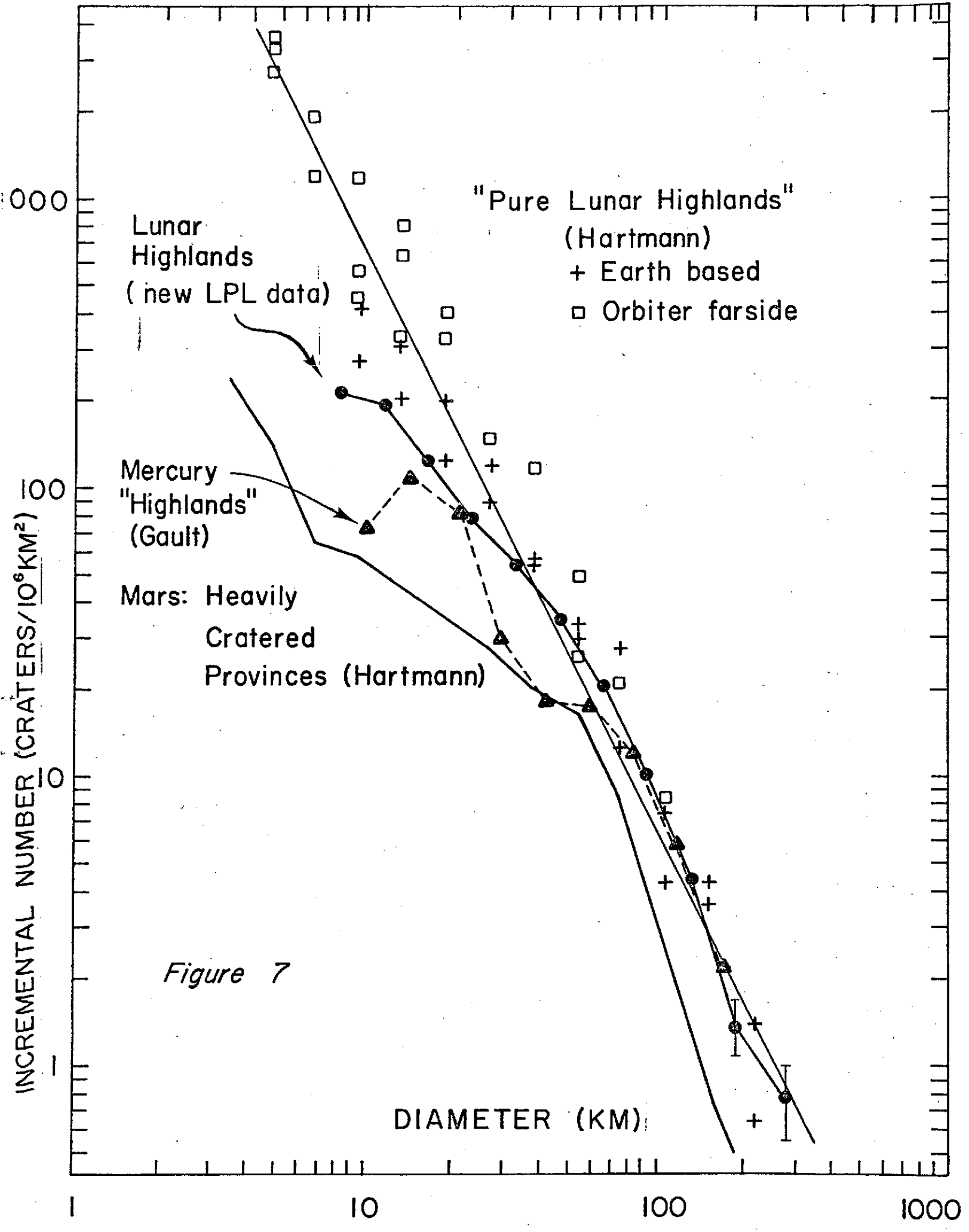
"Pure Lunar Highlands"
(Hartmann)
+ Earth based
□ Orbiter farside
Lunar
Highlands
(new LPL data)
Mercury
"Highlands"
(Gault)
Mars: Heavily
Cratered
Provinces (Hartmann)
INCREMENTAL NUMBER (CRATERS/10⁶KM²)
000
100
10
1
DIAMETER (KM)
1
10
100
1000

Figure 7

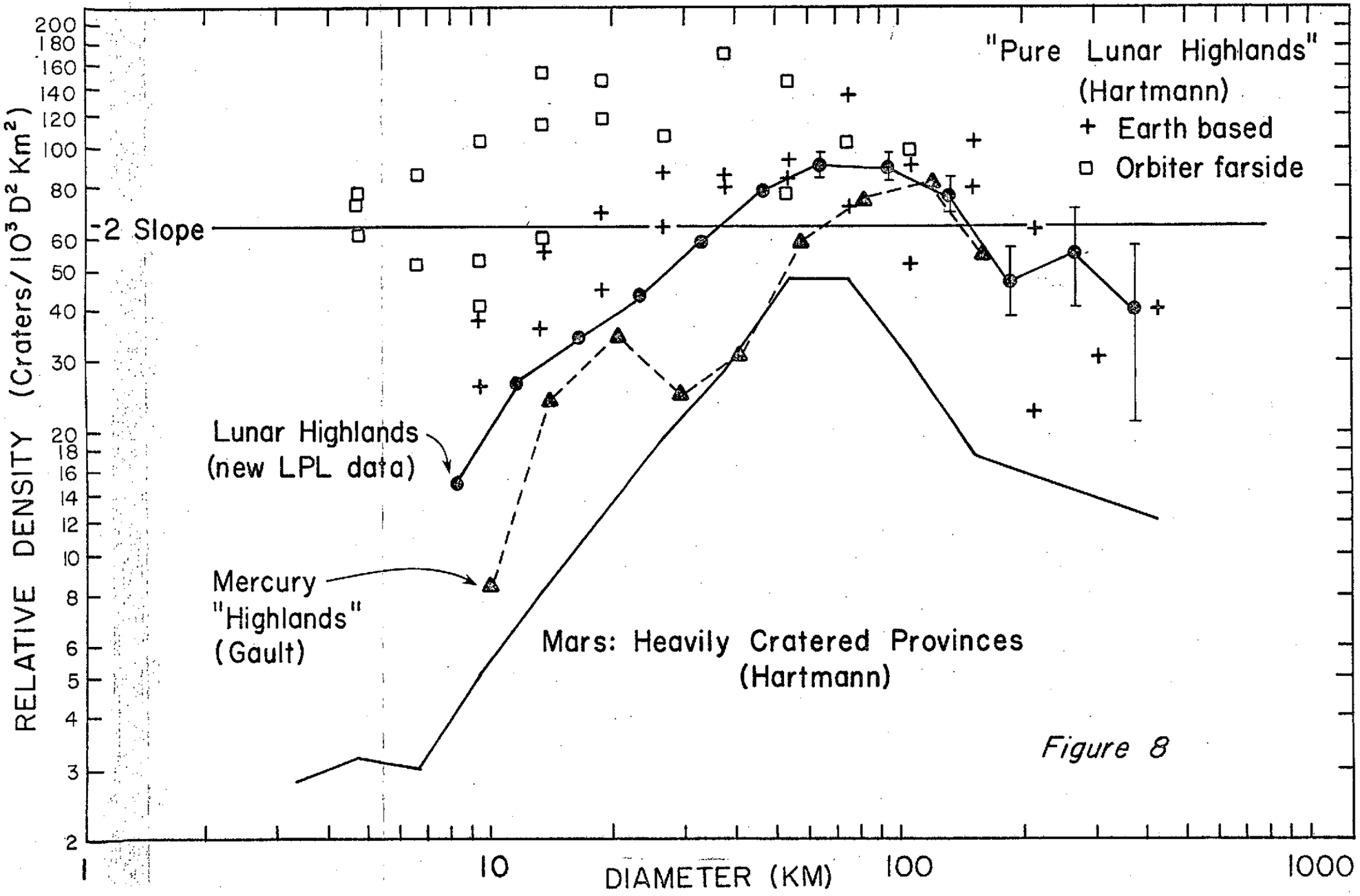
"Pure Lunar Highlands"
(Hartmann)
+ Earth based
□ Orbiter farside
-2 Slope
Lunar Highlands
(new LPL data)
Mercury
"Highlands"
(Gault)
Mars: Heavily Cratered Provinces
(Hartmann)
RELATIVE DENSITY (Craters/10³ D² Km²)
DIAMETER (KM)
200
180
160
140
120
100
80
60
50
40
30
20
18
16
14
12
10
8
6
5
4
3
2
1
10
100
1000

Figure 8

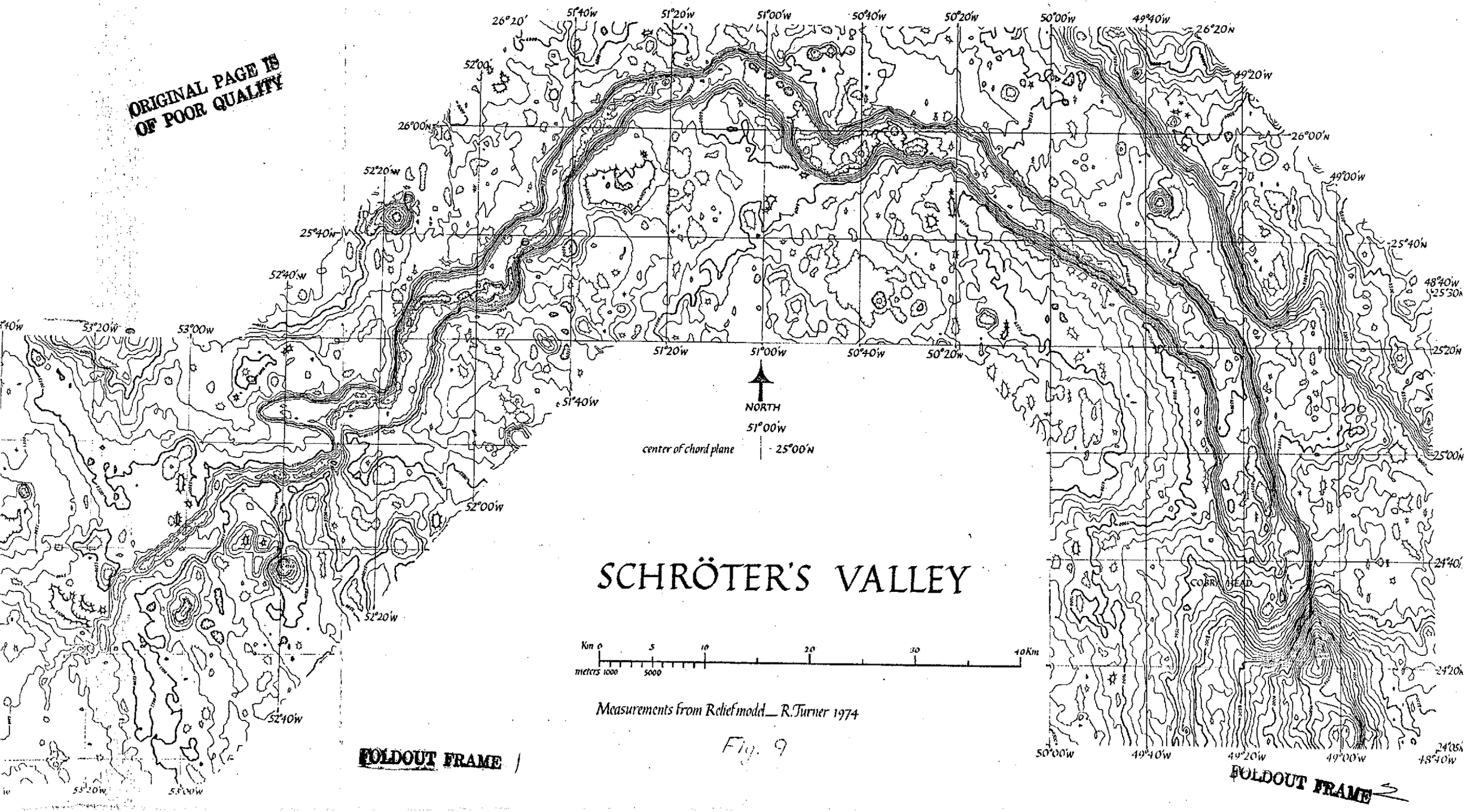

SCHRÖTER'S VALLEY

Measurements from Relief model_ R. Turner 1974

Fig. 9

FOLDOUT FRAME 1

FOLDOUT FRAME 2

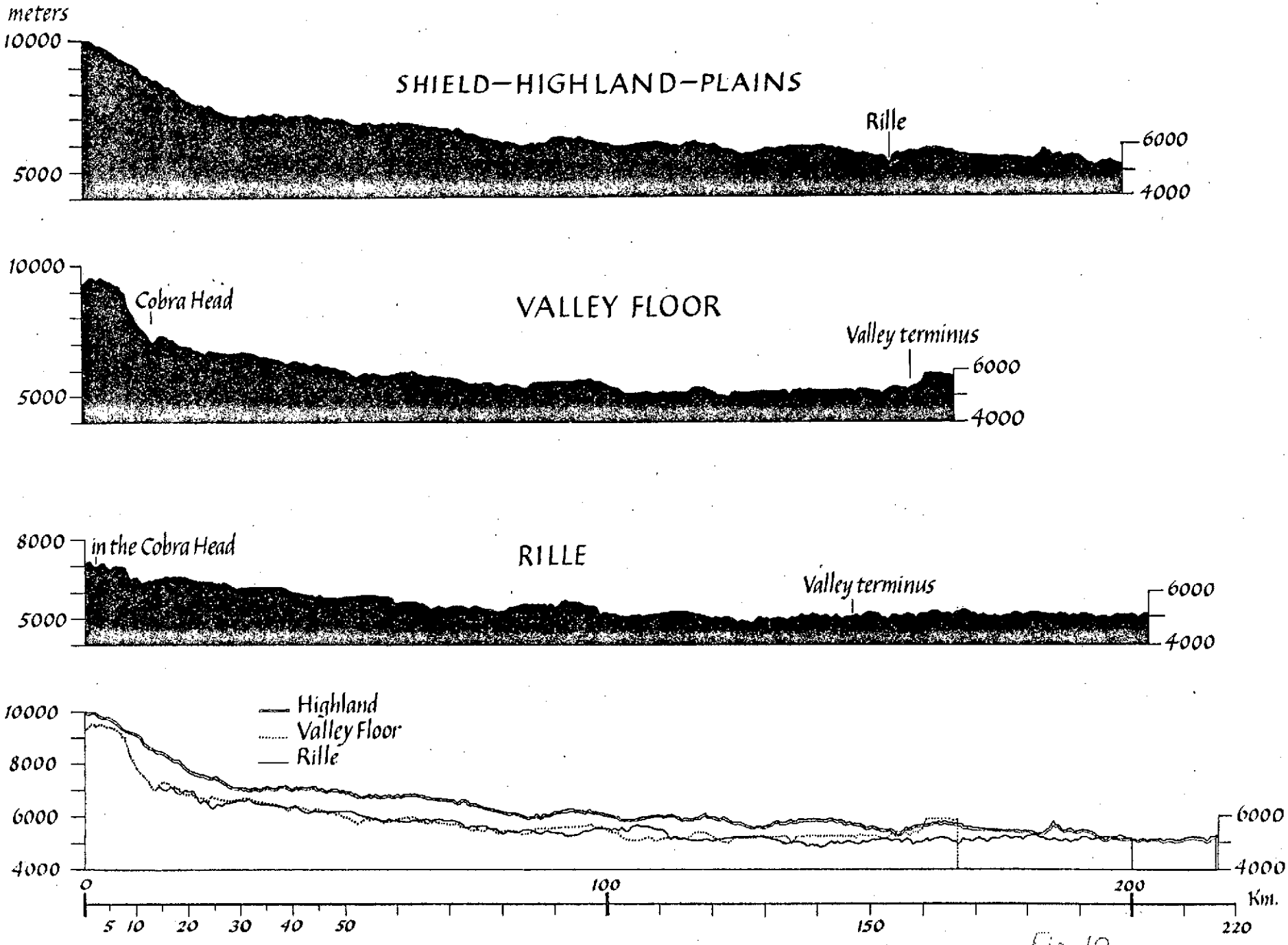
meters
10000
5000
SHIELD—HIGHLAND—PLAINS
Rille
6000
4000
10000
5000
Cobra Head
VALLEY FLOOR
Valley terminus
6000
4000
8000
5000
in the Cobra Head
RILLE
Valley terminus
6000
4000
10000
8000
6000
4000
Highland
Valley Floor
Rille
6000
4000
0
100
200
Km.
5
10
20
30
40
50
150
220

Fig. 10

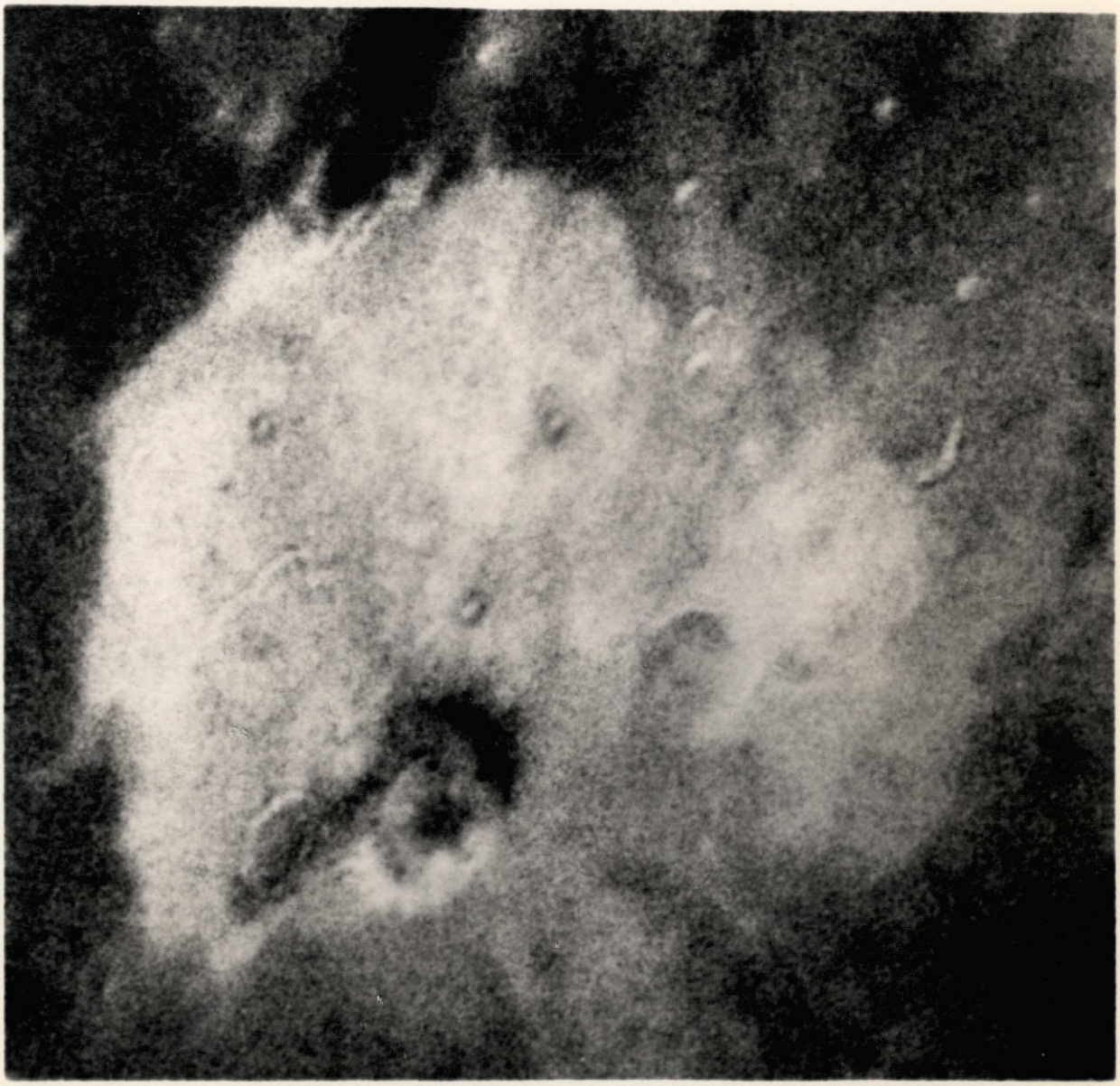

Color-difference photograph of Aristarchus-Wood's Spot region of Moon (red minus UV). Redder areas appear lighter.

Depth calculations for lunar craters from Orbiter photos.

(current method by L. Andersson)

The input data are:

for the photograph: spacecraft altitude a [km]
" longitude λ_n
" latitude β_n
" tilt angle T
" tilt azimuth A_z
Sun's colongitude $\overline{\tau}_o$
" latitude β_o

for the crater: coordinates of shadow casting point ξ, η
shadow length on photograph Σ' [see below for unit used]

Cartesian coordinates are in units of the Moon's mean radius R = 1738.1 km. Origin is at the Moon's center. ξ axis points towards East, η axis towards North, and ζ axis towards Earth. Shadow casting points are assumed to be on Moon's mean surface so that $\xi^2 + \eta^2 + \zeta^2 = 1$. All distances are in units of R except where specifically noted. The following subscripts will be used:

subscript	referring to
o	Sun or subsolar point
s	spacecraft
n	" nadir
P	principal point
Q	camera axis
none	crater (shadow casting point)

In the figures, a bar is used to indicate a complement angle (e.g. $\overline{\beta} = 90° - \beta$). The symbol N denotes the North pole, n the spacecraft nadir, s the spacecraft, 0 the center of the Moon, P the principal ground point, o the subsolar point, and C the crater (shadow casting point).

The following quantities are obtained directly from the input data:

$\rho = 1 + a/R$

$\xi_n = \rho \sin \lambda_n \cos \beta_n$

$\eta_n = \rho \sin \beta_n$

$\zeta_n = \rho \cos \lambda_n \cos \beta_n$

$\lambda_o = 90° - \overline{\lambda}_o$

$\xi_o = \sin \lambda_o \cos \beta_o$

$\eta_o = \sin \beta_o$

$\zeta_o = \cos \lambda_o \cos \beta_o$

$\zeta = \sqrt{1 - \xi^2 - \eta^2}$

$\lambda = \text{arctg } \xi/\zeta$

$\beta = \arcsin \eta$

Location of Sun with respect to crater (Fig. 1):

Sun's elevation angle = E_o

Sun's azimuth = A_o

$\sin E_o = \sin \beta \sin \beta_o + \cos \beta \cos \beta_o \cos (\lambda - \lambda_o)$ (cosine theorem on Δ CN$_o$)

$= \xi\xi_o + \eta\eta_o + \zeta\zeta_o$

$\sin A_o = \cos \beta_o \sin (\lambda - \lambda_o)/\cos E_o$ (sine theorem on Δ CN$_o$)

$\cos A_o = (\sin \beta_o - \sin \beta \sin E_o)/\cos \beta \cos E_o$ (cosine theorem on Δ CN$_o$)

Location of spacecraft with respect to crater (Figs. 2a and 2b):

Selenocentric angle between crater and spacecraft = g

Spacecraft azimuth = An

Spacecraft elevation angle = E_s

distance from crater to spacecraft = χ [units of R]

$$\cos g = \sin \beta \sin \beta_n + \cos \beta \cos \beta_n \cos (\lambda_n - \lambda) \quad \text{(cosine theorem on } \Delta \text{ CNn)}$$

$$= \xi\xi_n + \eta\eta_n + \zeta\zeta_n$$

$$\sin An = \cos \beta_n \sin (\lambda_n - \lambda)/\sin g \quad \text{(sine theorem on } \Delta \text{ CNn)}$$

$$\cos An = (\sin \beta_n - \sin \beta \cos g)/\cos \beta \sin g \quad \text{(cosine theorem on } \Delta \text{ CNn)}$$

$$\chi = \sqrt{1 + \rho^2 - 2\rho \cos g} \quad \text{(plane cosine theorem on } \Delta \text{ COs)}$$

$$\cos E_s = \rho \sin g/\chi \quad \text{(plane sine theorem on } \Delta \text{ COs)}$$

Relations between crater, spacecraft, and camera axis (Figs. 3a and 3b):

Let Q be the point whose coordinates are the direction cosines of the camera axis (the positive direction of which is taken to be from P to s).

Selenocentric angle between spacecraft and principal point = k

Slant range (distance between spacecraft and p.p.) = S [units of R]

angle between camera axis and position vector of crater = h

azimuth of Q at crater = A_Q

$$\sin \beta_Q = \cos T \sin \beta_n - \sin T \cos \beta_n \cos A_Z \quad \text{(cosine theorem on } \Delta \text{ QNn)}$$

$$\sin(\lambda_n - \lambda_Q) = \sin T \sin A_Z/\cos \beta_Q \quad \text{(sine theorem on } \Delta \text{ QNn)}$$

$$\cos(\lambda_n - \lambda_Q) = (\cos T - \sin \beta_n \sin \beta_Q)/\cos \beta_n \cos \beta_Q \quad \text{(cosine theorem on } \Delta \text{ QNn)}$$

$$\lambda_Q = \lambda_n - (\lambda_n - \lambda_Q)$$

$$\xi_Q = \sin \lambda_Q \cos \beta_Q$$

$$\eta_Q = \sin \beta_Q$$

$$\zeta_Q = \cos \lambda_Q \cos \beta_Q$$

$$S = \rho \cos T - \sqrt{1 - \rho^2 \sin^2 T} \qquad \text{(plane cosine theorem on } \Delta \text{ POs)}$$

$$\sin k = S \sin T$$

$$\sin \beta_P = \cos k \sin \beta_n + \sin k \cos \beta_n \cos A_Z \qquad \text{(cosine theorem on } \Delta \text{ PNn)}$$

$$\sin(\lambda_P - \lambda_n) = \sin k \sin A_Z / \cos \beta_P \qquad \text{(sine theorem on } \Delta \text{ PNn)}$$

$$\cos(\lambda_P - \lambda_n) = (\cos k - \sin \beta_n \sin \beta_P)/\cos \beta_n \cos \beta_P \qquad \text{(cosine theorem on } \Delta \text{ PNn)}$$

$$\lambda_P = \lambda_n + (\lambda_P - \lambda_n)$$

$$\xi_P = \sin \lambda_P \cos \beta_P$$

$$\eta_P = \sin \beta_P$$

$$\zeta_P = \cos \lambda_P \cos \beta_P$$

$$\cos h = \sin \beta \sin \beta_Q + \cos \beta \cos \beta_Q \cos(\lambda_Q - \lambda) \qquad \text{(cosine theorem on } \Delta \text{ CNQ)}$$

$$= \xi\xi_Q + \eta\eta_Q + \zeta\zeta_Q$$

$$\sin A_Q = \cos \beta_Q \sin(\lambda_Q - \lambda)/\sin h \qquad \text{(sine theorem on } \Delta \text{ CNQ)}$$

$$\cos A_Q = (\sin \beta_Q - \sin \beta \cos h)/\cos \beta \sin h \qquad \text{(cosine theorem on } \Delta \text{ CNQ)}$$

Linear distance between P and C = ℓ [units of R]
Angle at spacecraft between P and C = α (Fig. 4)
Angle between sun direction and camera axis = x (Fig. 5)

$$\ell^2 = (\xi-\xi_P)^2 + (\eta-\eta_P)^2 + (\zeta-\zeta_P)^2$$

$$\cos\alpha = (\chi^2 + S^2 - \ell^2)/2\chi S \qquad \text{(plane cosine theorem on } \Delta \text{ CPs)}$$

$$\cos x = \sin\beta_o \sin\beta_Q + \cos\beta_o \cos\beta_Q \cos(\lambda_Q-\lambda_o) \qquad \text{(cosine theorem on } \Delta \text{ QNo)}$$

Now consider Fig. 6. The Z-axis is the camera axis. The XY-plane, which we will call the "object plane", contains the point C (the shadow-casting point). The end (bottom) of the shadow is at K; the length of the shadow hypotenuse is σ. The projection of the shadow on the object plane is CL. The angle in the plane, at the crater, between this projection and JC (the projection of the spacecraft-crater line) is denoted by H. Finally, M is the intersection of JL and sK. The line CM, of length Σ, is the "apparent shadow length", which is in the same ratio to the distance spacecraft-object plane as is the length of the shadow image in the film plane to the focal length of the camera.

Let the distance LJ be = t, LM = p, and the angle JLC = γ. Then:

$$t^2 = \sigma^2 \sin^2 x + \chi^2\sin^2\alpha + 2\sigma\chi \sin x \sin\alpha \cos H \qquad \text{(plane cosine theorem on } \Delta \text{ JCL)}$$

$$\sin\gamma = \chi \sin H \sin\alpha/t \qquad \text{(plane sine theorem on } \Delta \text{ JCL)}$$

$$\frac{p}{t-p} = \frac{\sigma \cos x}{\chi \cos\alpha} \qquad (\Delta \text{ JsM} \backsim \Delta \text{ LMK})$$

$$\Sigma^2 = p^2 + \sigma^2 \sin^2 x - 2p\sigma \sin x \cos\gamma \qquad \text{(plane cosine theorem on } \Delta \text{ CLM)}$$

Combining these four equations, eliminating p, t, and γ, yields after some manipulation:

$$\Sigma^2 = \frac{\chi^2\sigma^2(\cos^2\alpha \sin^2 x + \sin^2\alpha \cos^2 x - 2 \sin x \cos x \sin\alpha \cos\alpha \cos H)}{(\sigma \cos x + \chi \cos\alpha)^2}$$

$$\Rightarrow \quad \sigma = \frac{\Sigma\chi \cos\alpha}{\chi G - \Sigma \cos x} \quad , \text{ where } G = \sqrt{\sin^2(x+\alpha) - \frac{1+\cos H}{2} \sin 2x \sin 2\alpha}$$

To obtain σ in kilometers, χ and Σ must be converted to this unit.

$$\chi_{km} = 1738.1\chi$$

$$\Sigma_{km} = 1738.1 \frac{\Sigma'}{f} \chi \, a \cos\alpha$$

(Since in Fig. 6 Js may be thought of as the camera's focal length, f, and Σ as the shadow length in the film plane, Σ')

Here a is the ratio of the scale of the spacecraft film to the scale of the prints used for the shadow measurements. a = 0.1380 is the adopted value.

Thus

$$\sigma_{km} = \frac{1738.1\chi}{\frac{G}{\cos\alpha} \frac{f}{a\Sigma'} - 1}$$

Let the altitude of the shadow casting point over the mean surface of the Moon be δ (Fig. 7), the depth of the crater d, and the previously derived elevation angle of the Sun E_o. Then

$$(R + \delta - d)^2 = (R + \delta)^2 + \sigma^2 - 2(R + \delta)\sigma \sin E_o \qquad \text{(plane cosine theorem)}$$

$$d = (R + \delta)\left(1 - \sqrt{1 - 2\frac{\sigma \sin E_o}{R + \delta} + \left(\frac{\sigma}{R + \delta}\right)^2}\right)$$

Expanding in a series one obtains

$$d = \sigma \sin E_o - \frac{\sigma^2}{2R}\cos^2 E_o + \frac{\sigma^2}{4R^2}\cos^2 E_o(\sigma \sin E_o + 2\delta) + \ldots.$$

Since δ is generally unknown, but small (of the order of d), it is appropriate to retain two and only two terms of the expansion:

$$\boxed{d = \sigma \sin E_o - \frac{\sigma^2}{2R}\cos^2 E_o}$$

Fig. 1

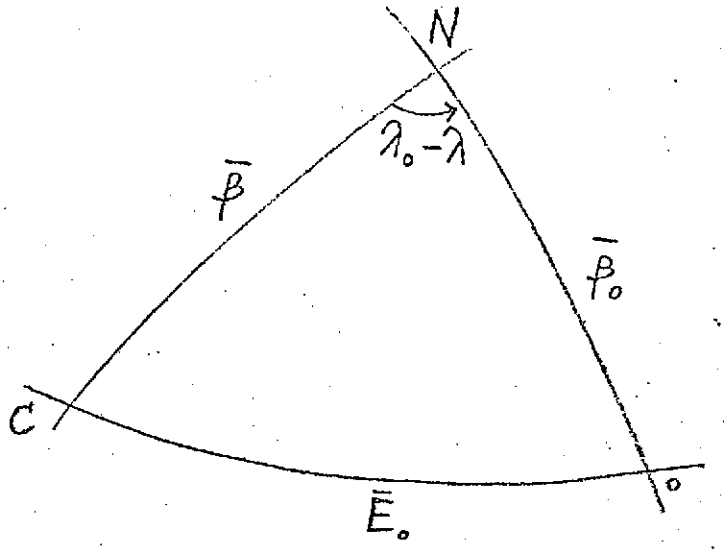

Fig. 2a

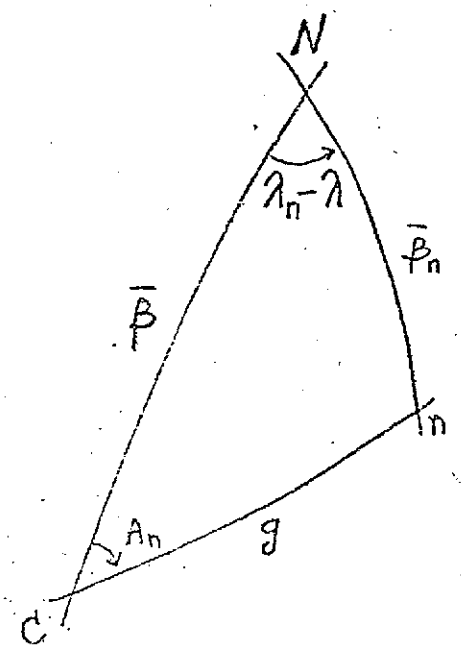

Fig. 2b

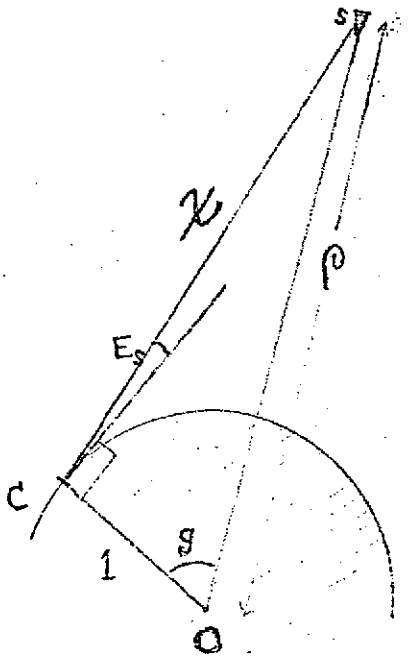

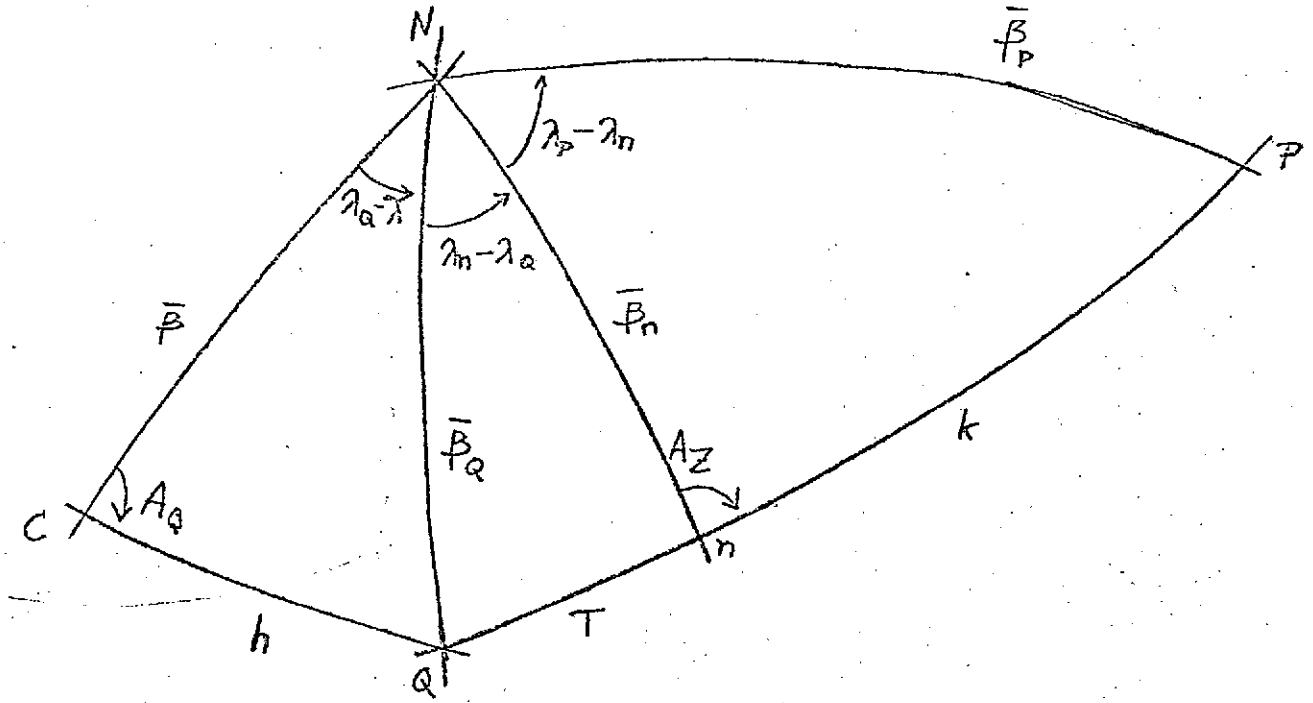

Fig. 3 a

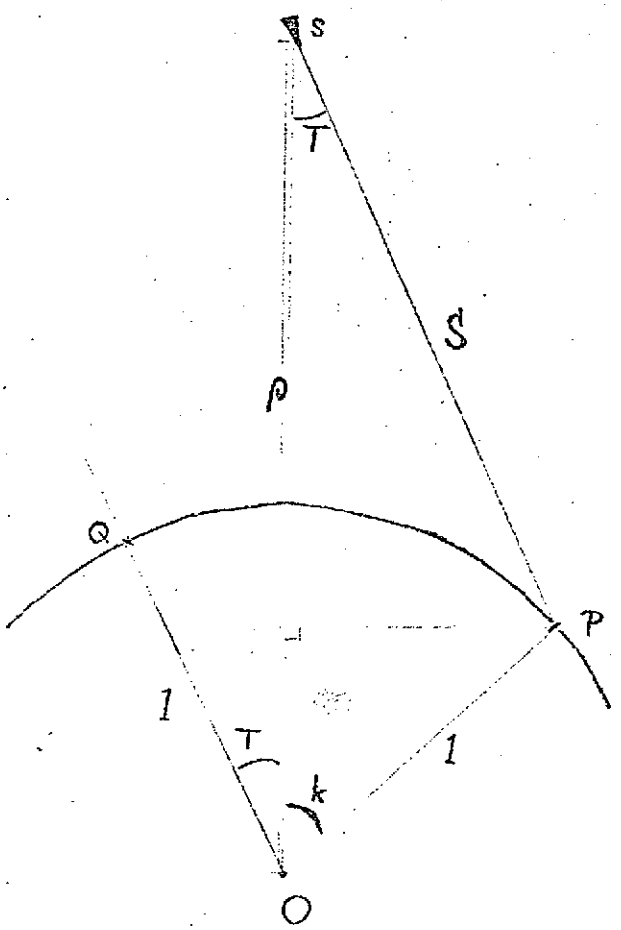

Fig. 3 b

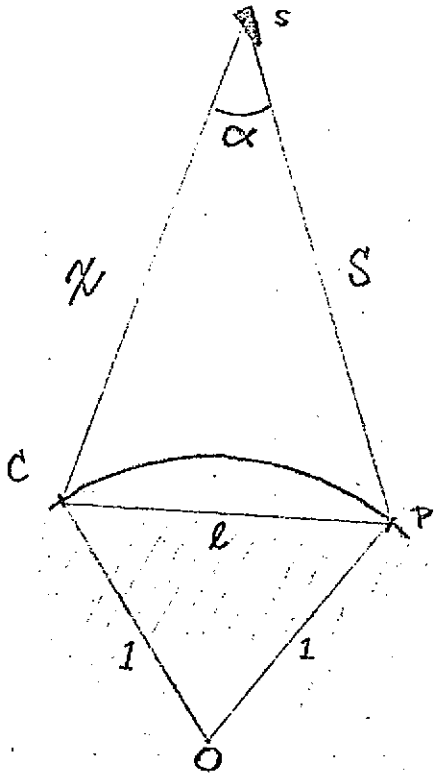

Fig. 4

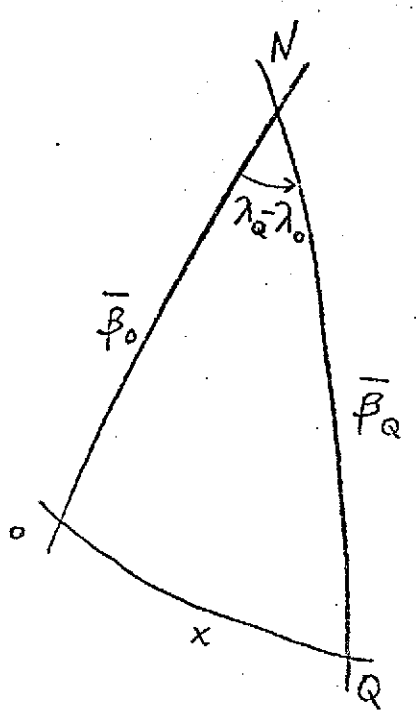

Fig. 5

Fig. 6

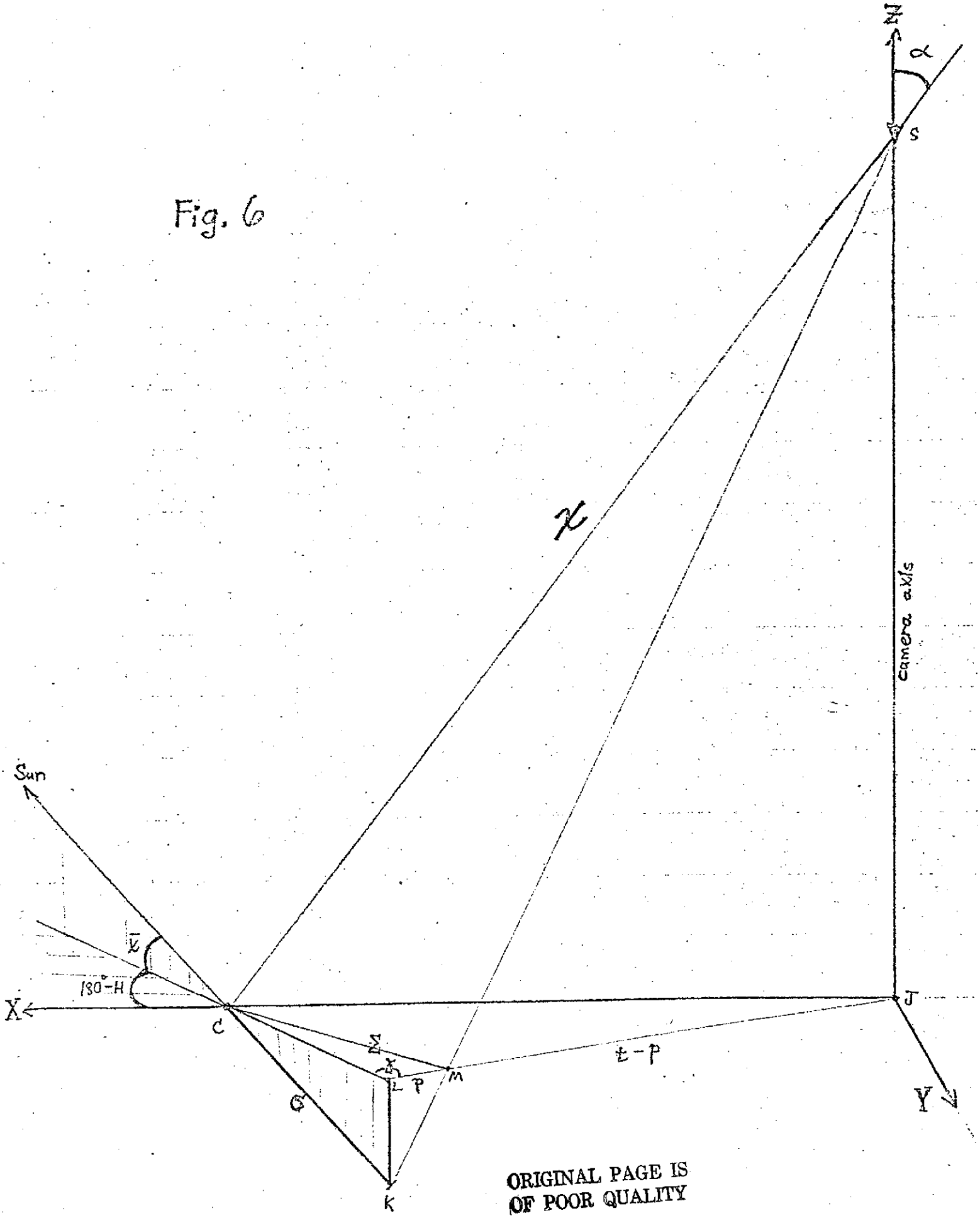

Fig. 7